A Comparison of Sea Ice Dynamics Models at High Resolution

E. C. HUNKE

Group T-3, Los Alamos National Laboratory, Los Alamos, New Mexico

Y. ZHANG

Oceanography Department, Naval Postgraduate School, Monterey, California

(Manuscript received 10 January 1998, in final form 24 March 1998)

ABSTRACT

An elastic-viscous-plastic (EVP) model for sea ice dynamics has recently been proposed as a computationally efficient alternative to the viscous-plastic (VP) model widely in use. The EVP model features a fully explicit discretization that improves the model's efficiency, particularly on high-resolution grids, and adapts easily to parallel computation. Comparison of two high-resolution Arctic sea ice simulations, identical except for the ice dynamics, indicates that the EVP model reproduces the VP model behavior on timescales relevant to climate studies. The ice concentration and thickness distributions over a 1-yr integration period are remarkably similar in the two models, although the EVP model responds more rapidly and accurately to strong synoptic weather systems than does the VP model, compared to drifting Arctic buoys. A close look at rates of strain shows that elastic waves in the EVP model do not significantly alter the ice behavior in highly compact areas, where the waves most benefit numerical efficiency. Internal stress of the ice is also similar in the two models; both deviate from viscoplasticity in regions of nearly rigid ice and in regions of low concentration undergoing approximately free drift motion.

1. Introduction

Arctic ice forms primarily along the Siberian coast and in open leads throughout the ice pack. Ice transits the western Arctic in one of two prominent, large-scale movements: it flows away from Siberia toward the North Pole with the Transpolar Drift Stream, or it revolves around the Beaufort Gyre, an anticyclonic circulation in the Canada Basin. Ice finally exits the Arctic basin through the Fram Strait and a web of narrow passages in the Canadian Archipelago (Colony and Thorndike 1984; Barry et al. 1993). Because of this movement across the ocean surface, the thermodynamic consequences of sea ice are felt throughout the polar oceans and indeed globally. For example, brine rejection during freezing is believed to be an important mechanism for the formation of bottom water and for the thermohaline circulation (Aagaard and Carmack 1989; Yang and Neelin 1993).

Therefore, climate simulations of the Arctic region require both an appropriate model for the ice dynamics and a highly resolved mesh in order to capture the ice circulation patterns properly. A nonlinear viscous-plastic rheology proposed by Hibler (1979) has become the standard sea ice dynamics model, but numerical implementations of this model suffer from difficulties related to the presence of an enormous range of effective viscosities. Its large computational requirements become particularly cumbersome on finely resolved grids or when the sea ice model is coupled to an ocean or atmosphere model (Hibler and Bryan 1987; Oberhuber 1993a,b).

The viscous-plastic rheology has been modified by Hunke and Dukowicz (1997) to include a computationally efficient elastic wave mechanism as a numerical regularization of the singularity that occurs at zero strain rate. This leads to a fully explicit discretization scheme, which is a great advantage in parallel architectures. In contrived test problems, the elastic-viscous-plastic rheology has been demonstrated to reproduce viscous-plastic model behavior on long timescales while producing more accurate ice response to physical forcing on shorter timescales (Hunke and Dukowicz 1997). Here we present a comparison of the viscous-plastic (VP) and elastic-viscous-plastic (EVP) models in a realistic, high-resolution simulation of Arctic sea ice and compare the simulated ice motion fields to that of drifting Arctic buoys.

Section 2 describes the model design and mathemat-

Corresponding author address: Dr. Yuxia Zhang, Oceanography Department, Naval Postgraduate School, Code OC/Zh, Monterey, CA 93943.
E-mail: zhangy@meeker.ucar.edu

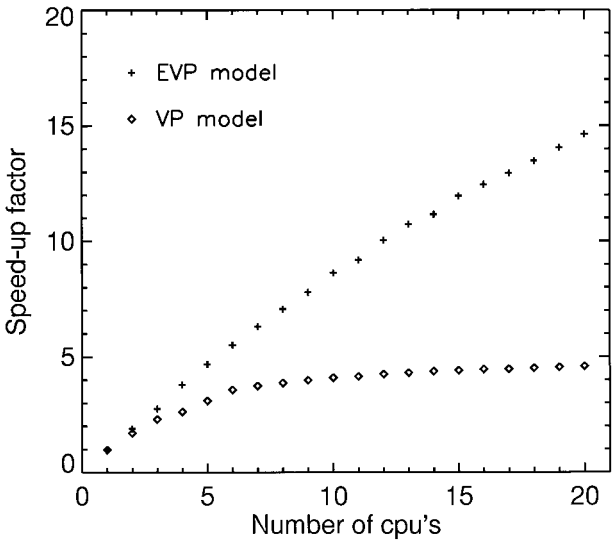

FIG. 1. Estimated dedicated performance for the EVP and VP models on a 20-processor Cray Research system.

ical differences between the two dynamics formulations and compares their computational performance. Rates of strain and internal stress of the ice are discussed in section 3 for both simulations, along with ice concentration and velocity, and a case study illustrates differences that occur between the models' ice motion fields on short timescales. The results of the comparison are summarized in section 4. In short, the simulations are quite similar on long timescales, but the EVP model responds more quickly to changing winds than does the VP model. The EVP model is also considerably more efficient on the multiprocessor computer used here.

2. Model specifications

a. Design

The comparison simulations are framed within a dynamic–thermodynamic sea ice model with identical domains, initializations, and forcing fields. The thermodynamic component consists of the zero-layer approximation of Semtner (1976) with an energy budget at the ice surface following Parkinson and Washington (1979). The dynamics component of the VP model uses the semi-implicit algorithm of Zhang and Hibler (1997), but with Jacobi iteration replacing their successive overrelaxation technique. This allows the VP code to be vectorized and reduces the computer time by a factor of 2 over the successive overrelaxation method. Both simulations employ the advection scheme of Hibler (1979).

The 300 × 360 square mesh has a resolution of 1/6°, or about 18 km. Initial ice conditions were obtained with the VP model, run for 6 yr with 1992 European Centre for Medium-Range Weather Forecasts (ECMWF) atmospheric forcing from an initially uniform, 2-m-thick slab of ice. For both the initial spinup and the comparison simulations, the sea ice models were forced from below with output every 3 days from an ocean model, which was driven by 1992 ECMWF atmospheric data that had been averaged and interpolated to the model timestep of 4 h. The simulations described below were driven by 6-hourly ECMWF atmospheric

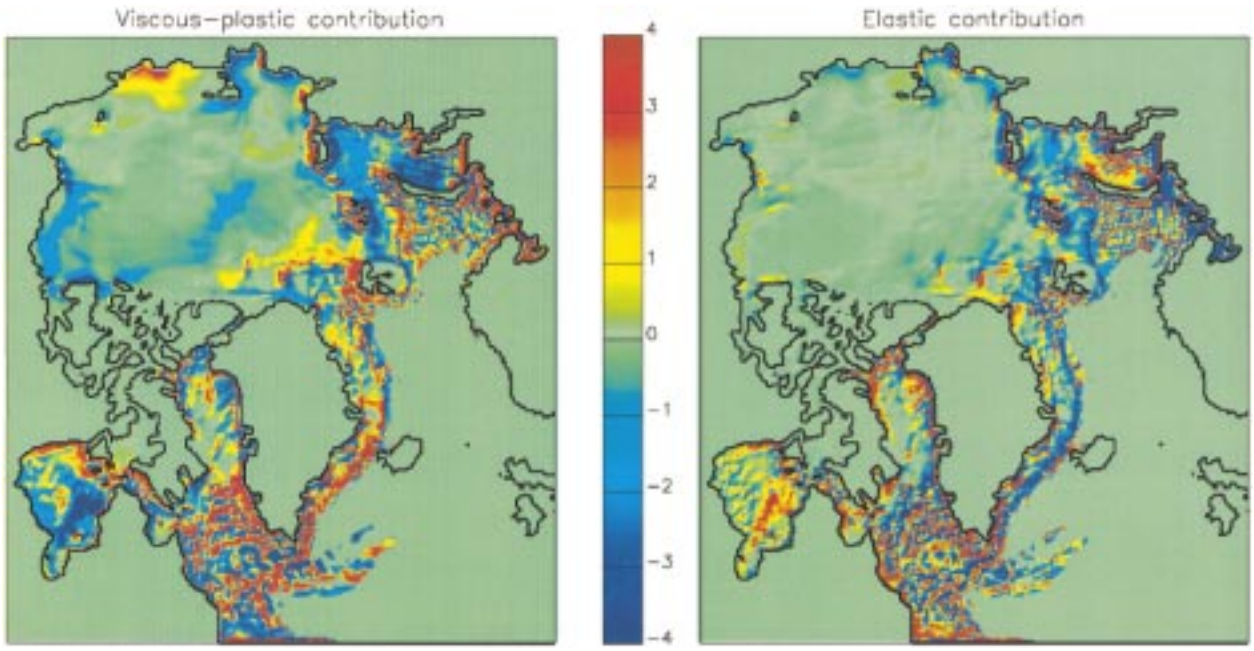

FIG. 2. Viscous-plastic and elastic contributions to the EVP model ice divergence for 7 February 1990, in units of 10^{-7} s^{-1}.

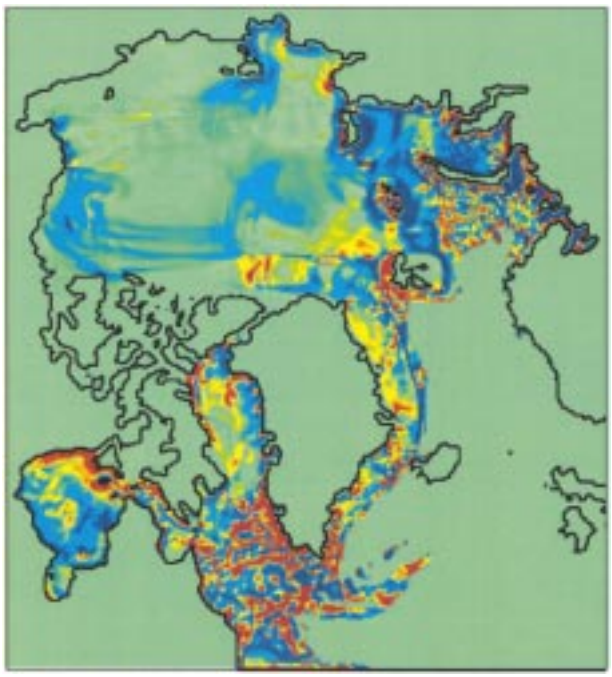

FIG. 3. VP model ice divergence for 7 February 1990. The scale is the same as in Fig. 2.

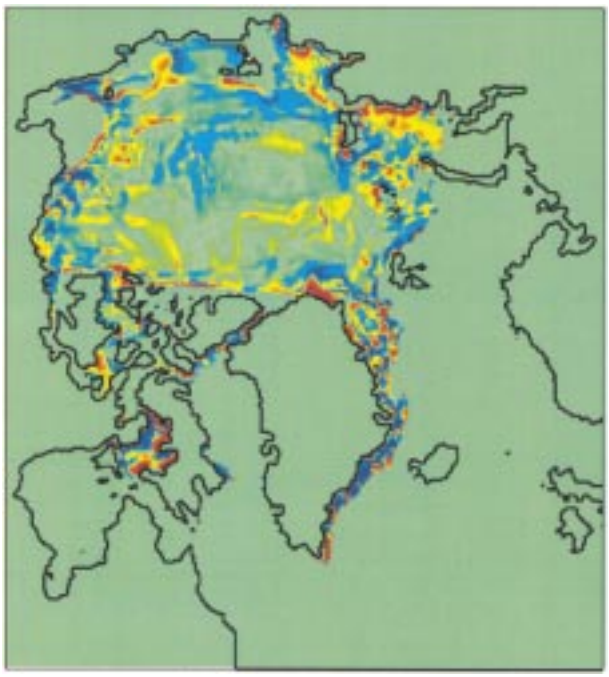

FIG. 5. VP model ice divergence for 5 September 1990. The scale is the same as in Fig. 4.

data for 1990, averaged every 3 days and linearly interpolated to the time step as above.

b. Ice rheology

The force balance per unit area in the ice pack is given by a two-dimensional momentum equation,

$$m\frac{\partial u_i}{\partial t} = \frac{\partial \sigma_{ij}}{\partial x_j} + \tau_i(u_i), \tag{1}$$

where τ_i depends nonlinearly on the ice velocity u_i and represents external forcing on the ice due to wind and ocean stresses, sea surface slope, and Coriolis effects.

The strength of the ice is represented by the internal

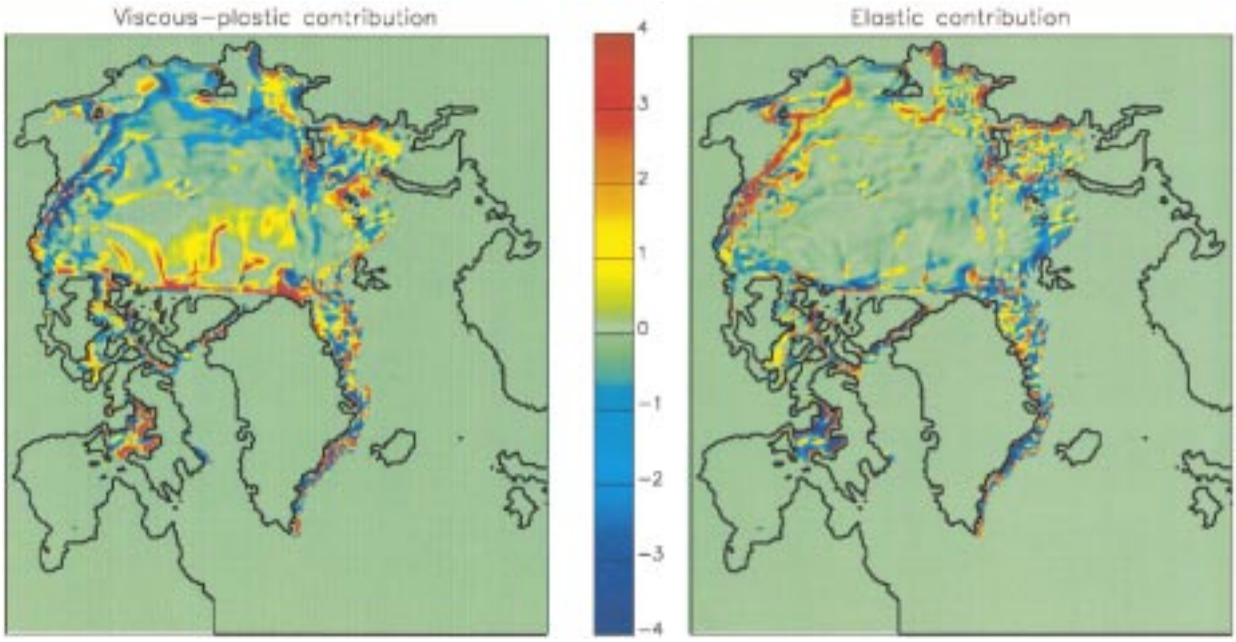

FIG. 4. Viscous-plastic and elastic contributions to the EVP model ice divergence for 5 September 1990, in units of 10^{-7} s^{-1}.

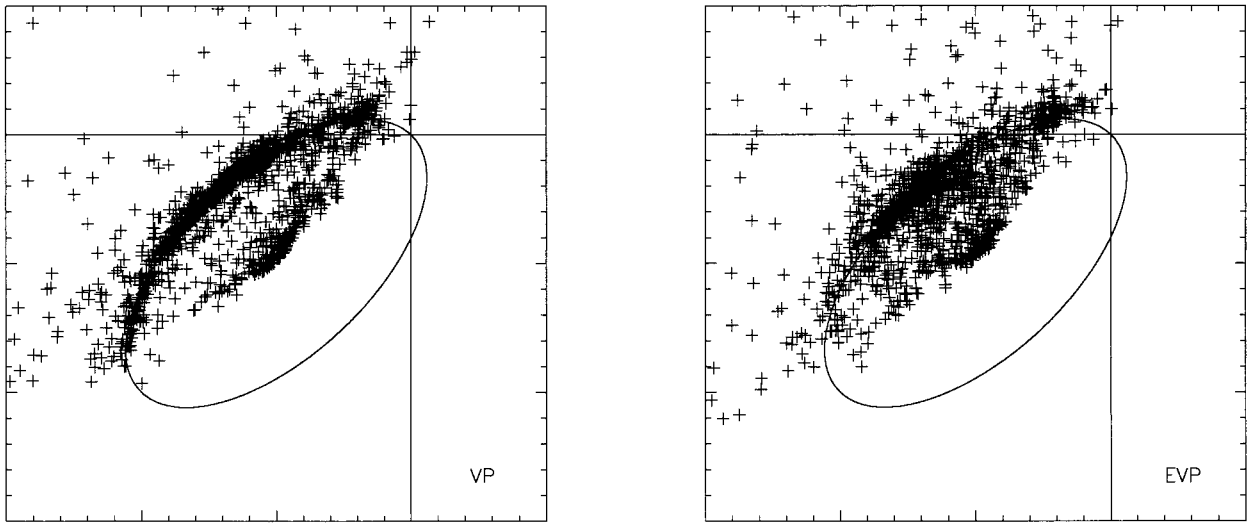

FIG. 6. Normalized principal ice internal stresses on 7 February 1990.

stress tensor σ_{ij}. The viscoplastic rheology proposed by Hibler (1979) is given by a constitutive law that relates the internal ice stress σ_{ij} and the rates of strain $\dot{\epsilon}_{ij}$ through an internal ice pressure, P, and nonlinear bulk and shear viscosities, ζ and η, such that the principal components of stress lie on an elliptical yield curve with the ratio of major to minor axes e equal to 2. This constitutive law is given by

$$\frac{1}{2\eta}\sigma_{ij} + \frac{\eta - \zeta}{4\eta\zeta}\sigma_{kk}\delta_{ij} + \frac{P}{4\zeta}\delta_{ij} = \dot{\epsilon}_{ij}, \tag{2}$$

where

$$\dot{\epsilon}_{ij} = \frac{1}{2}\left(\frac{\partial u_i}{\partial x_j} + \frac{\partial u_j}{\partial x_i}\right). \tag{3}$$

This is easily inverted to give the stress σ_{ij} as a function of the strain rate $\dot{\epsilon}_{ij}$.

The viscosities are defined in terms of the strain rates, becoming infinite in the limit of zero strain rate:

$$\zeta = \frac{P}{2\Delta},$$

$$\eta = \frac{P}{2\Delta e^2},$$

$$\Delta = [(\dot{\epsilon}_{11}^2 + \dot{\epsilon}_{22}^2)(1 + e^{-2}) + 4e^{-2}\dot{\epsilon}_{12}^2 + 2\dot{\epsilon}_{11}\dot{\epsilon}_{22}(1 - e^{-2})]^{1/2}.$$

To regularize this behavior, Hibler (1979) set upper bounds for the viscosities that depend on the ice thickness and concentration. Thus, when the ice pack is rigid (e.g., fast ice near a coast or a large, solid floe floating in the central pack), it is treated as a linear viscous fluid undergoing very slow creep. A lower bound is also set for the viscosities, and the two bounds may differ by five orders of magnitude. Furthermore, the time step restriction for explicit discretization of the viscous-plastic equations is proportional to $\Delta x^2/\zeta$, where Δx is the mesh size, necessitating use of implicit methods for time steps larger than a few seconds in regions of nearly rigid ice, particularly on high-resolution grids.

The VP ice rheology therefore consists of the viscoplastic constitutive law, strain rates, and viscosities defined as above, and the linear viscous regularization for extreme values of viscosity.

Hunke and Dukowicz (1997) present an alternative regularization, the introduction of elastic waves. The regularization is accomplished by adding an elastic contribution to the strain rate:

$$\frac{1}{E}\frac{\partial\sigma_{ij}}{\partial t} + \frac{1}{2\eta}\sigma_{ij} + \frac{\eta - \zeta}{4\eta\zeta}\sigma_{kk}\delta_{ij} + \frac{P}{4\zeta}\delta_{ij} = \dot{\epsilon}_{ij}, \tag{4}$$

where E is a parameter corresponding to Young's modulus. By a proper choice of parameters and time discretization, the time step restriction can be made to depend *linearly* on Δx, and its dependence on ζ can be removed altogether. Thus, this formulation can be discretized explicitly with an acceptably long time step, a great advantage for implementations on parallel machines and highly resolved grids.

As described in Hunke and Dukowicz (1997), the VP model suffers a large linearization error in its time discretization, which weakens or delays its transient response to rapidly changing conditions. The EVP model uses a subcycling scheme to estimate velocity gradients within the VP time step, which improves the transient response of the solution and leads to more accurate behavior in the EVP model. Note that at steady state the elastic term in (4) disappears. Subcycling takes the EVP solution toward steady state on each time step; enough subcycling reproduces the VP model behavior exactly, as the elastic waves damp out. Thus, the elastic term

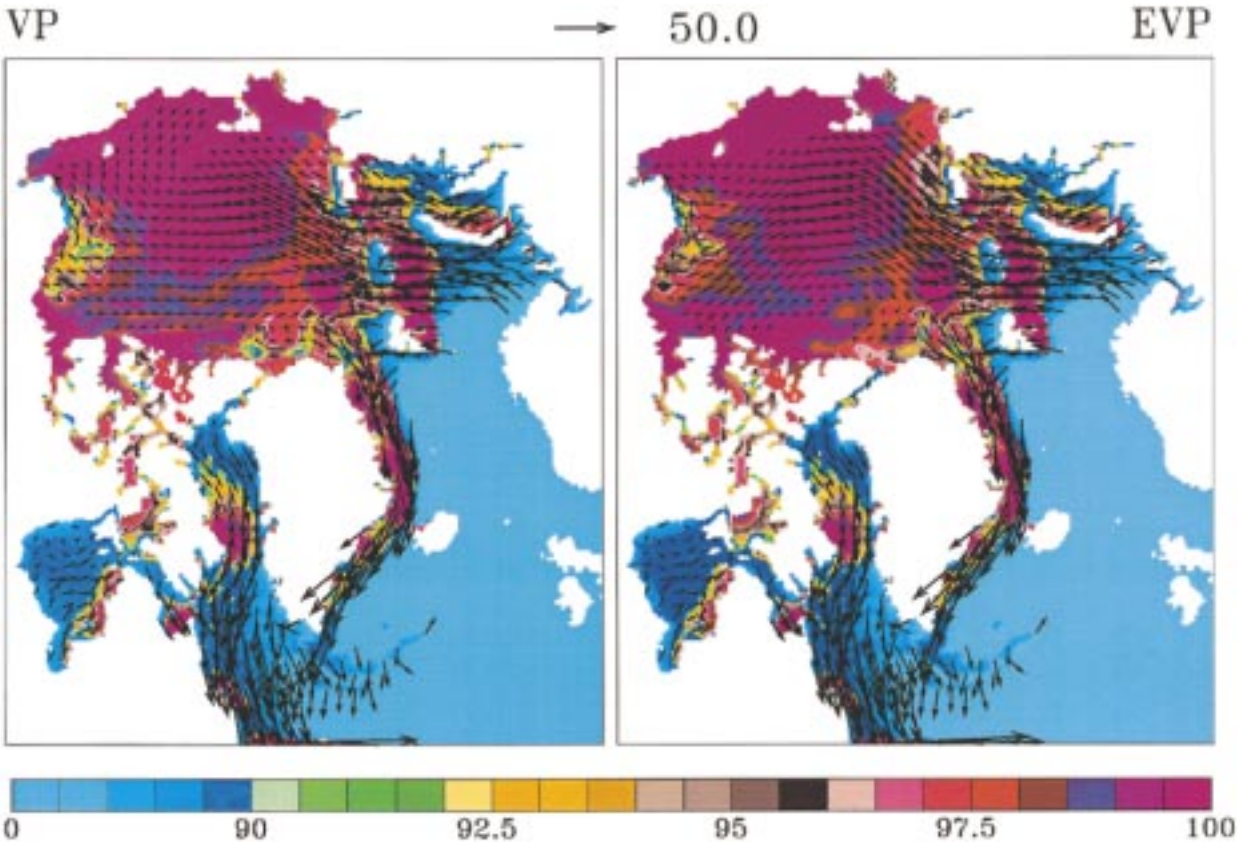

FIG. 7. Ice concentration distributions (%) on 7 February 1990, overlaid with instantaneous velocity vectors (cm s^{-1}) from the VP and EVP models. The color scale has been adjusted to emphasize differences in regions of high concentration.

initially makes a ''prediction'' for the stress σ_{ij}, which is then ''corrected'' toward the VP solution during the subcycling. We take advantage of this by choosing the number of subcycles N small enough that the EVP solution adjusts quickly to rapidly changing forcing conditions, yet large enough that the elastic waves do not alter the VP solution significantly on longer timescales. Here, $N = 100$. For additional details about the EVP ice dynamics model, see Hunke and Dukowicz (1997).

c. Computational efficiency

The original purpose of developing the EVP model was to improve the efficiency of the VP numerical model. The numerical methods used here for the VP model effect a twofold improvement in unitasking performance over the method of Zhang and Hibler (1997), due to improved vectorization of the decoupled momentum equations with Jacobi iteration as opposed to successive overrelaxation. The EVP model is an additional 30% faster than the (Jacobi) VP model in terms of total CPU time needed.

Because it is discretized explicitly, the EVP model performs significantly better on multiprocessor machines. The simulations described here were autotasked on a Cray J90 series computer with 20 CPUs. Figure 1 shows estimated dedicated performance of the EVP and VP numerical models as a function of the total number of processors used. The speedup factor (wallclock serial time/parallel time) for the VP model's performance increases with up to six dedicated processors. Using more than six dedicated processors does not further improve the VP model's performance. The EVP model's performance scales better, meaning that when the two models are autotasked on a given number of dedicated processors, the EVP model runs much faster in terms of wallclock time than the VP model. (The data in Fig. 1 were generated by the software tool ATExpert, which predicts speedups on a dedicated Cray Research system based on data collected from a single run on a nondedicated system.)

3. Results

The viscous-plastic sea ice model has been validated by numerous researchers (e.g., Hibler and Walsh 1982; Hibler and Ackley 1983; Preller and Posey 1989; Kreyscher et al. 1997). We wish to highlight differences between the EVP and VP dynamics models and discuss their effects on the simulations, rather than validating

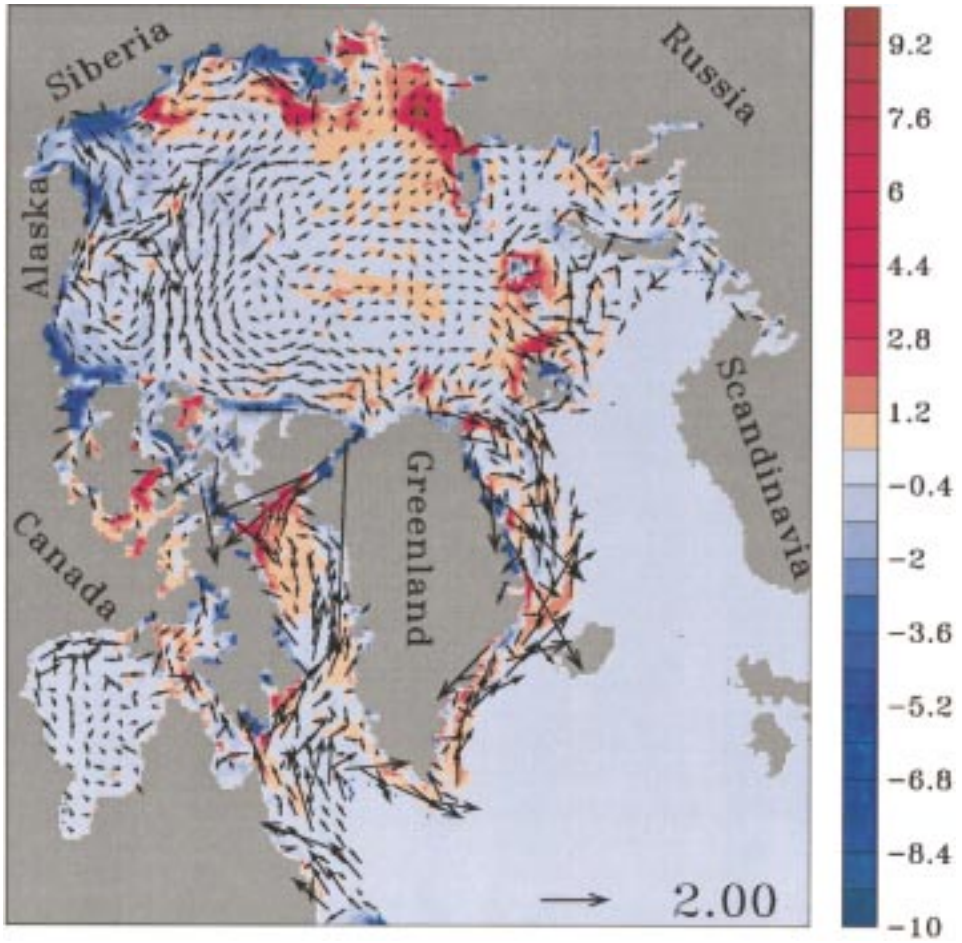

FIG. 8. The difference (EVP − VP) of annual mean sea ice concentration (%) and velocity (cm s^{-1}).

either simulation against observations, although we do include some observed buoy data to illustrate synoptic-scale motion of Arctic ice.

We compare the EVP and VP simulations by first investigating the most fundamental difference between the two models, represented by the rate of strain tensors in (2) and (4). We then present ice concentration distributions from the simulations, discuss seasonal vari-

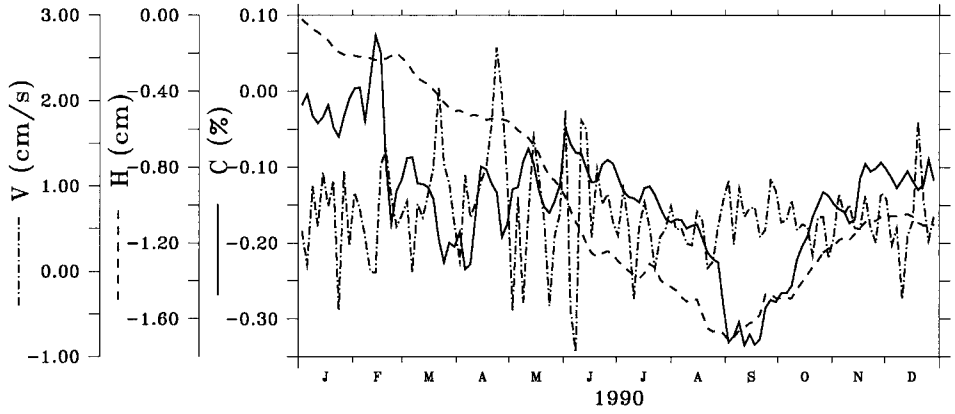

FIG. 9. EVP − VP differences of areal-averaged ice velocity (V), effective thickness (H), and compactness (c). Averages were taken over the ice-covered area.

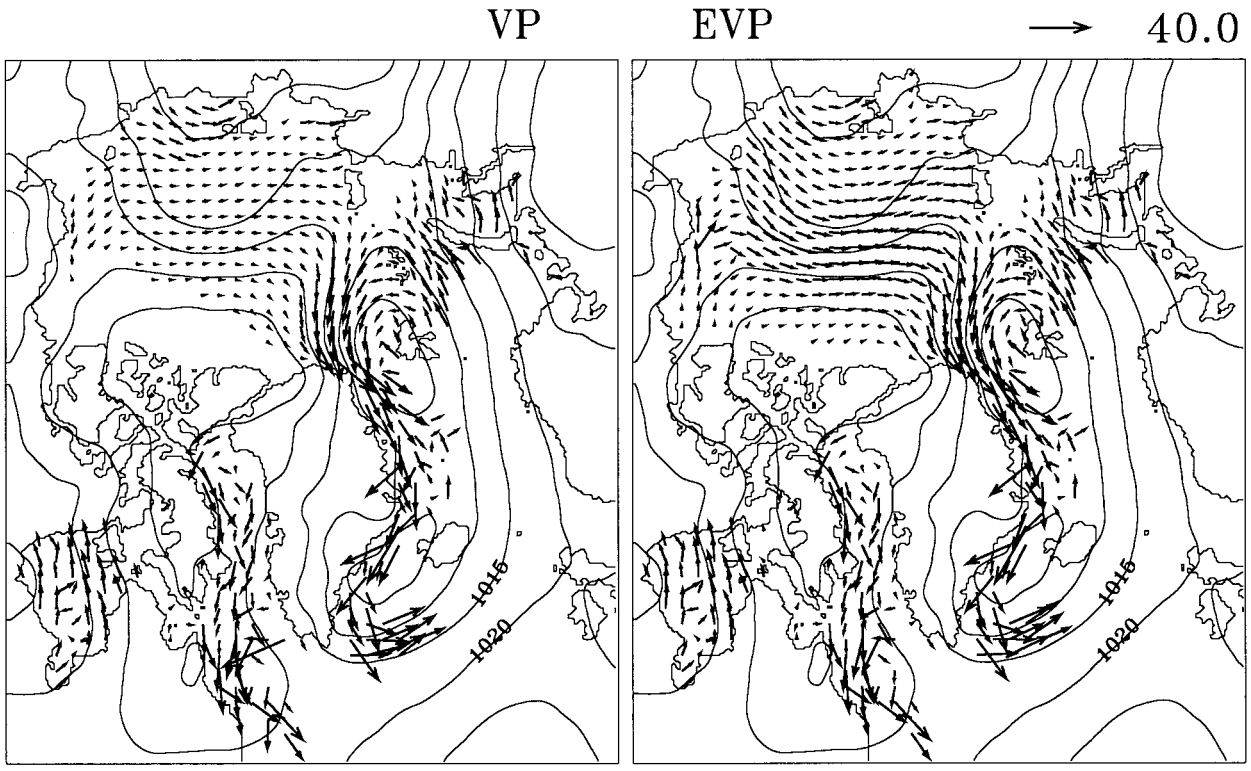

FIG. 10. Atmospheric surface pressure (mb) and ice velocities (cm s^{-1}) for 23 April 1990, from the VP and EVP simulations.

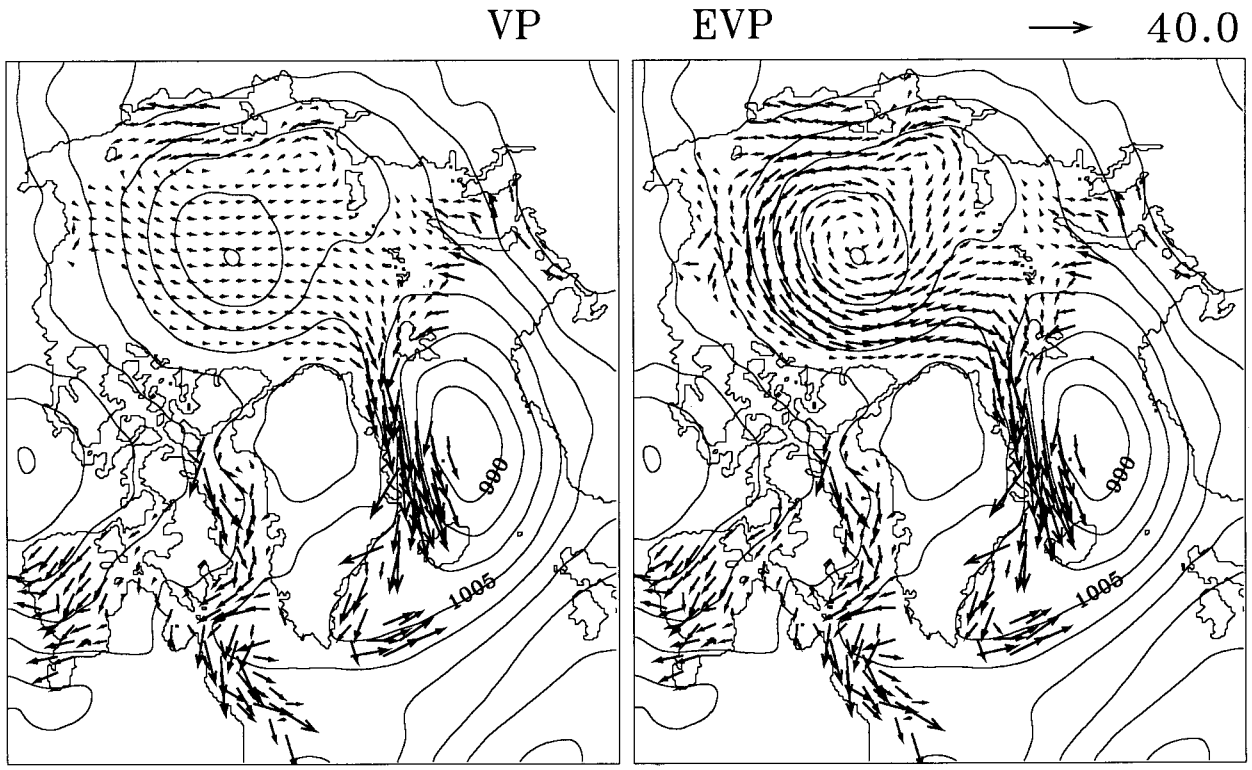

FIG. 11. Atmospheric surface pressure (mb) and ice velocities (cm s^{-1}) for 26 April 1990, from the VP and EVP simulations. The EVP ice motion responds quickly to the strong low pressure system in the central basin, unlike the VP simulation.

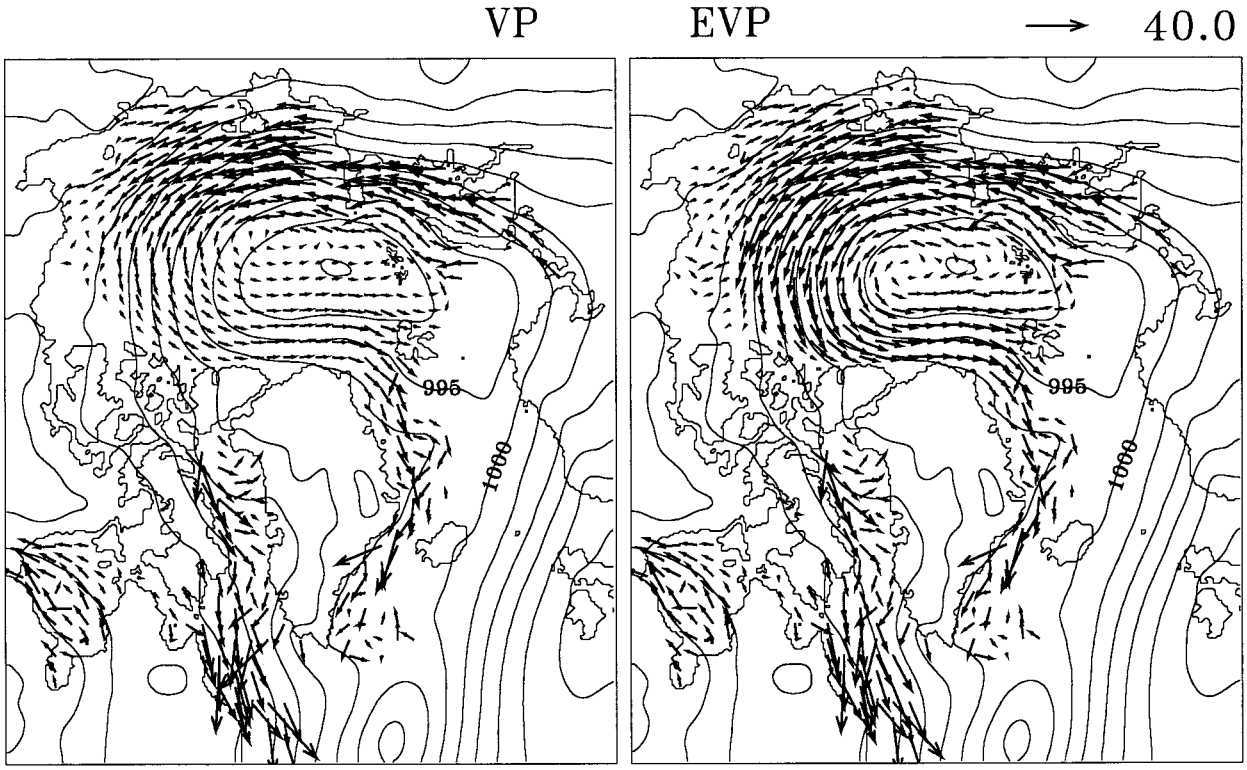

FIG. 12. Atmospheric surface pressure (mb) and ice velocities (cm s^{-1}) for 29 April 1990, from the VP and EVP simulations. The VP simulation now responds to the low pressure system, but the center of the ice circulation is closer to the low pressure center on 26 April (Fig. 11).

ations, and present a case study that illustrates the difference in the model response to surface forcing on timescales of less than a week.

a. Rates of strain

The ice pack is a heterogeneous mixture of open water and various thicknesses of ice. The deformation of a parcel of this mixture can be decomposed into changes in its volume, given by divergence or convergence of the ice, and changes in its shape due to shearing forces. The two invariants of the strain rate tensor (3), namely, its trace and determinant, characterize these changes independent of coordinate axes, allowing output from the two runs to be compared directly. Here we focus on the trace of the strain rate tensor, which gives the ice divergence. The other invariant, $\dot{\epsilon}_{11}\dot{\epsilon}_{22} - \dot{\epsilon}_{12}^2$, has similar characteristics in the two simulations to the divergence fields and is not shown.

The rate of strain tensor on the right-hand side of (4) consists of both elastic and viscous-plastic contributions: $\dot{\boldsymbol{\epsilon}}_{ij} = \dot{\boldsymbol{\epsilon}}_{ij}^{e} + \dot{\boldsymbol{\epsilon}}_{ij}^{vp}$, where

$$\dot{\boldsymbol{\epsilon}}_{ij}^{e} = \frac{1}{E}\frac{\partial \sigma_{ij}}{\partial t},$$

and $\dot{\boldsymbol{\epsilon}}_{ij}^{vp}$ is given by (2). Figure 2 shows the contributions of the elastic and viscous-plastic components to the EVP ice divergence. The viscous-plastic contribution, $\boldsymbol{\nabla} \cdot \mathbf{u}^{vp} = \dot{\boldsymbol{\epsilon}}_{11}^{vp} + \dot{\boldsymbol{\epsilon}}_{22}^{vp}$, is calculated during the model run using (2), and the elastic contribution is then given by $\boldsymbol{\nabla} \cdot \mathbf{u}^{e} = \boldsymbol{\nabla} \cdot \mathbf{u} - \boldsymbol{\nabla} \cdot \mathbf{u}^{vp}$, where $\boldsymbol{\nabla} \cdot \mathbf{u}$ is the total EVP divergence. The corresponding ice divergence field for the VP model is shown in Fig. 3.

Rates of strain, and therefore divergence and convergence, are large near the ice edge in both models, because of low ice strength associated with either low compactness or small thickness. The viscosities take minimum values and the ice in this region is linear viscous. The scale in Figs. 2 and 3 has been artificially cut off at $\pm 4 \times 10^{-7}$ s^{-1}, so that smaller variations in the interior of the ice pack are visible.

The central pack is highly compact in February, and the EVP viscous-plastic contribution to the ice divergence is remarkably similar to the VP model's. Although elastic waves in the EVP model are most effective at ice concentrations over 80% (Hunke and Dukowicz 1997), the elastic contribution is quite small in the central Arctic. Similarly, very small divergence in the Canadian Archipelago reflects the highly compact sea ice in both models. In this region the VP model is in the linear viscous regime with maximal viscosities, and elastic waves are active in the EVP model. Velocity magnitudes are so small, however, that significant differences between the model simulations do not appear.

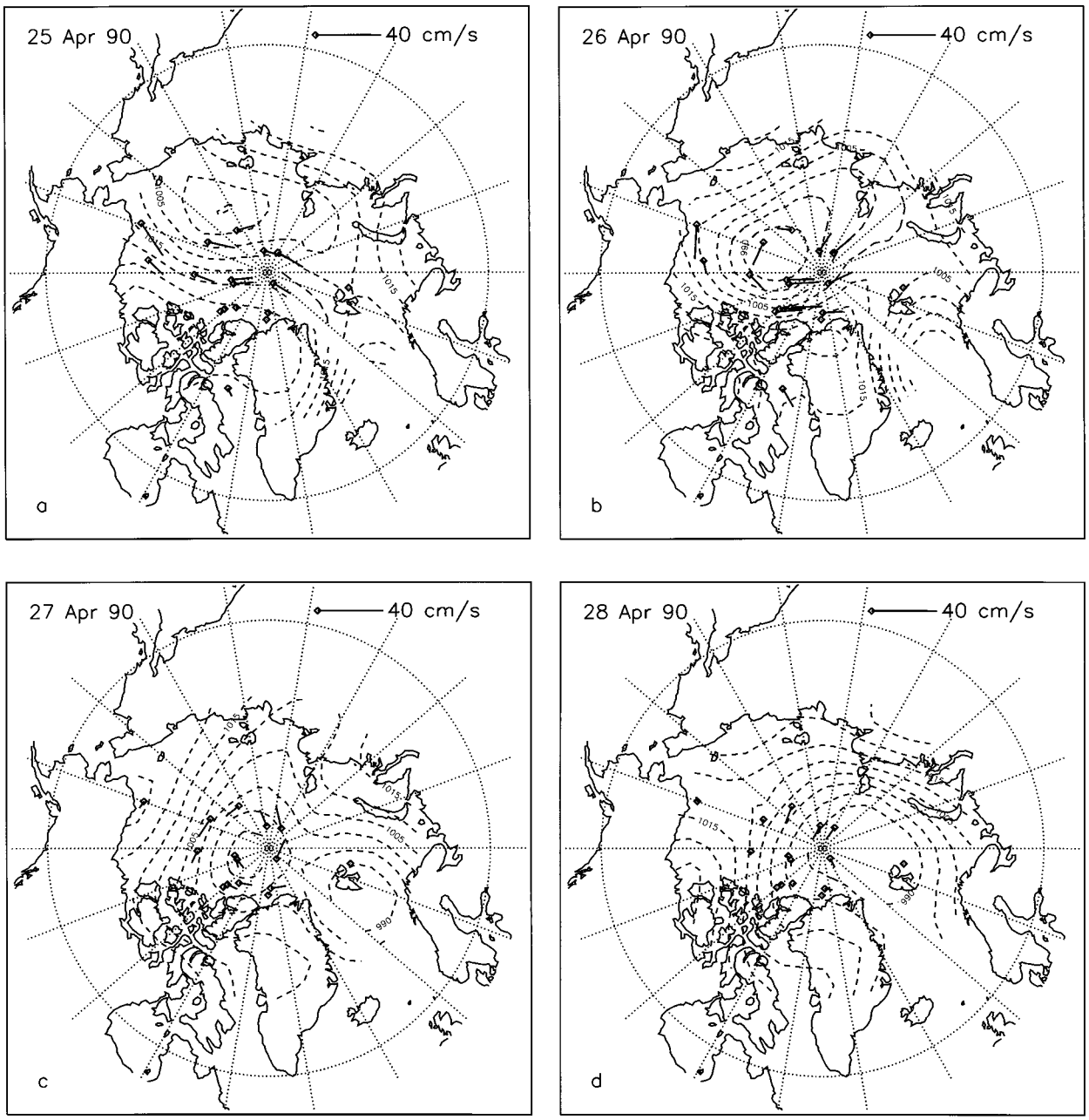

FIG. 13. Arctic buoy drifts and pressure fields (mb) during the April 1990 case study period [(a)–(d) 25–28 April 1990]. Diamonds indicate the buoy position at 0000 UTC and the tail represents the net motion during that day. Buoy drift directions change quickly in response to the changing wind pattern.

The ice pack is less compact in the Arctic summer, and the ice edge moves into the central basin. These changes are evident in the divergence fields for 5 September 1990, shown in Figs. 4 and 5. Viscous-plastic strain rates in both models reveal a great deal of finely structured ice motion in the central basin.

These figures are meant to illustrate the essential difference between the VP and EVP models, the elastic waves themselves. The net ice divergence in the EVP model is partitioned between the viscous-plastic contribution and that due to elastic waves, such that the sum approximately equals the VP model divergence. This is primarily achieved by the two contributions taking opposite signs, so that where the viscous-plastic contribution is divergent, the elastic contribution is convergent, and vise versa. We see that the elastic waves are largely damped in areas of compact ice. Thus, the net EVP ice divergence (not

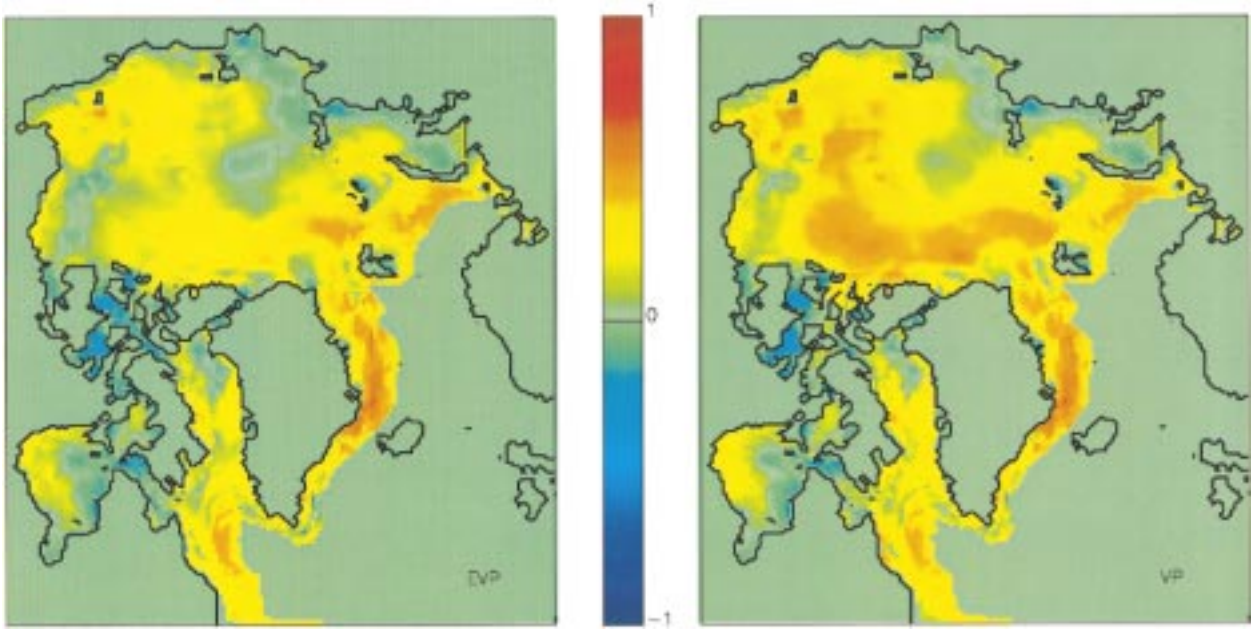

FIG. 14. Linear correlation coefficients between ice speeds and geostrophic wind speeds 3 days earlier. The VP-model ice motion is more highly correlated with past winds than is the EVP model.

shown) is nearly indistinguishable from the viscous-plastic contribution alone and is also quite similar to the VP model ice divergence.

b. Ice internal stress

A sampling of the principal stress components (computed from σ_{ij}) in the central Arctic is shown in Fig. 6 for the VP and EVP models. If the simulated ice were moving as a perfect viscoplastic material, then all of the stresses would lie on the elliptical yield curve. Regularization of the constitutive law causes the stresses to stray from the yield curve. In particular, where the viscosities are at the maximum level in the VP model, the ice is treated as a linear viscous material and the stress falls inside the plastic yield curve. Thus, stresses in the Canadian Archipelago, where the ice is fairly rigid, tend to fall inside the ellipse.

Linearization of the stress tensor term in (1) lags the viscosities in time, causing additional departures from an elliptic yield curve. If the VP model were integrated to steady state before the forcing fields are updated, then the simulated ice would be perfectly plastic except where the viscosities have reached their minimum or maximum levels. That is, additional iterations or ''pseudo–time steps'' (Zhang and Hibler 1997) between forcing updates reconcile most simulated stresses with the elliptical yield curve.

The EVP model, on the other hand, has introduced elasticity to the viscoplastic material ice properties, which also causes departures from plastic behavior. Recall that increased subcycling modifies the EVP solution toward the VP numerical solution. Therefore, if the EVP subcycling were continued until the elastic waves completely damped out on each time step, and if the model were integrated to steady state before each forcing update, then the EVP ice would be a perfectly plastic material, except where the viscosities are extreme.

Through simplified test problems, Hunke and Dukowicz (1997) have shown that, despite departures from the yield curve, elastic waves in the EVP model enhance ice response to changing forcing conditions by allowing better estimates of ice velocities at each time step. This behavior is exhibited in the present, more realistic model runs discussed in section 3d.

TABLE 1. Linear correlation coefficients between ice motion and the geostrophic wind, averaged over the ice-covered area.

Model	Sync. wind	Lagged wind
	Speed	
EVP	0.67	0.16
VP	0.63	0.22
	Direction	
EVP	0.13	0.013
VP	0.10	0.024

c. Ice distribution

Differences in the VP and EVP velocity fields are traceable to the different ice dynamics models. However, the ice strength provides a feedback mechanism between the ice motion field and the ice concentration and thickness distributions; the cumulative effect of this mech-

anism obscures the connection between differences in the dynamics models and differences in the ice simulations. Ice extent and distribution are critical factors in the polar climate because of the high reflective and insulating properties of sea ice, and therefore differences in the simulations of ice concentration by the two models are of great concern.

In general, the EVP and VP ice distributions are strikingly similar, as illustrated in Fig. 7, which shows ice concentration and velocity fields for 7 February 1990. The color scale has been adjusted to emphasize differences for concentrations above 90%; the two concentration fields are indistinguishable otherwise.

Vectors indicating the difference in annually averaged velocities for the two models are shown in Fig. 8, overlying the difference of mean sea ice concentrations. The largest velocity differences occur near the ice edge; differences in the central pack are generally small. The EVP model exhibits a stronger Beaufort Gyre in the western Arctic basin, which is displaced toward Alaska in both models, but weaker ice motion in the Greenland and Labrador Seas and Baffin Bay.

Figure 8 indicates that the Arctic pack ice concentration is fairly robust to variations in the velocity fields. Concentration differences occur primarily along coasts and in regions of summer meltback. Differences in the thickness distributions are also small, generally less than 0.5 m (not shown).

The model simulations show the greatest disagreement in summer, as indicated by Fig. 9. Barely distinguishable in the winter months, the areal averaged EVP thickness and concentration differ from the VP results in the summer months by 13% and 7%, respectively, with less ice in the EVP simulation than in the VP simulation. The velocity differences between the models are smaller during summer and fall than the rest of the year. (Comparison of 5-yr simulations using 1990–94 data, not shown, indicates that the EVP − VP differences evident at the end of 1990 in Fig. 9 do not continue to grow. We will discuss interannual variations in a future publication.)

Ice motion is strongly dependent on variability in the atmospheric forcing, and correlations between ice motion and geostrophic winds have been demonstrated to be especially high in summer, when pack ice floes are drifting somewhat freely and the ice rheology is less influential (Thorndike and Colony 1982; Steele et al. 1997). Thus, the simulated ice motion fields are more similar during the summer months. Larger differences in ice concentration and thickness indicate that the feedback between ice motion and distribution is stronger in summer than in winter, when the ice is more compact. For example, heightened summer melting associated with enhanced slip lines in the central Arctic EVP ice pack (Fig. 4) contributes to lower ice concentrations in summer than that produced by the VP model (Tremblay and Mysak 1997). Likewise, the velocity–concentration feedback is stronger near the less compact ice edge than in the central pack, as illustrated in Fig. 8.

d. Transient response

The rates at which the two models respond to the imposed surface forcing strikingly illustrate the differences in the models. For example, Fig. 9 indicates that a large velocity difference occurs between the two simulations in late April. During this period a strong low pressure system passed across the Arctic, illustrated in Figs. 10–12. On 23 April (Fig. 10), velocities in the central Arctic are weak in the VP simulation as compared to the EVP ice motion field, while ice in both models follows the strong southwestward flow from the North Pole toward Greenland. By 26 April (Fig. 11) a low pressure system developed and moved into the western Arctic basin. It then drifted northward, as shown in Fig. 12. The VP ice does not develop a cyclonic gyre associated with the low pressure system until 29 April, and its center is displaced toward Siberia from the low pressure center's track. In contrast, ice motion in the EVP simulation adjusts quickly to the changing wind pattern. Velocity vectors from the EVP simulation follow the geostrophic wind, represented by the pressure contours, much more closely than the VP velocities.

Ice in the central Arctic has been observed to respond quickly to changing wind conditions; Campbell (1965) notes that floe ice obtains a steady-state motion within a few hours after a change of wind stress. Drifting buoys also exhibit this behavior. Figure 13 shows buoy drift vectors for 25–29 April, computed from data obtained from the International Arctic Buoy Programme, Polar Science Center, Seattle. The diamonds represent the buoy positions at 0000 UTC of the given date, and the tail indicates the net direction and relative speed of motion for that day. Interpolated buoy pressure fields at 1200 UTC, overlaid on each plot, show the low pressure center passing across the Arctic basin. The drifting buoys clearly change direction in response to shifting winds within 24 h of the shift, demonstrating that the EVP model's transient response is physically more accurate than the VP model's.

The VP model's response to the geostrophic wind lags behind the EVP model throughout the year. Figure 14 shows correlation coefficients between the ice speed (S) and the wind speed *3 days earlier* (W), calculated at each grid point according to

$$r = \frac{\sum_{k=1}^{N} (S_k - \overline{S})(W_k - \overline{W})}{\sqrt{\sum_{k=1}^{N} (S_k - \overline{S})^2} \sqrt{\sum_{k=1}^{N} (W_k - \overline{W})^2}},$$

where $N = 120$ is the number of data frames in one year and the overbar denotes the annual mean. Figure 14 demonstrates that the VP ice motion is more closely correlated with the earlier winds than is the EVP ice

motion, especially where the ice concentrations are relatively high year round. Table 1 provides mean correlation coefficients for the VP and EVP ice motion and the winds, averaged over the ice-covered area. While both models are correlated with the synchronous winds, the EVP correlation coefficient is greater than the VP model's, due primarily to the lag illustrated in Fig. 14. Correlations between the ice and wind directions also reflect the lagged response of the VP model.

The VP model's slow response to changes in the winds, which shows up both as lower ice speeds and different vector orientations from the EVP model, is due to the numerical discretization error discussed in Hunke and Dukowicz (1997). They have shown that this error is most egregious in regions of ice concentration above 80%, and the problem is significantly worse for concentrations above 90%. In the present simulations, the pack ice concentration in the central Arctic is 95% and higher at the end of April.

4. Discussion

We have demonstrated, in a high-resolution simulation of Arctic sea ice, that the EVP and VP ice dynamics models produce equivalent ice behavior, particularly on timescales longer than a week. Differences on shorter timescales tend to average out over time, so that climate simulations with the two models should be comparable.

Differences in the concentration and thickness distributions appear mainly at the ice edge and in the summer, both of which have lower concentrations in general. Because ice strength decreases as the ice becomes less compact, differences in the two dynamics models become less important; the EVP and VP dynamics both reduce to linear-viscous ''free drift'' descriptions, and the resulting ice motion is very similar in the two models. However, the ice distributions disagree more in less compact areas, suggesting that the feedback between ice velocity and ice concentration is stronger in times and regions where the ice concentration is lower: a given velocity difference between the models leads to larger variations between the ice distributions where ice is less compact.

Disparities between the models also appear when the wind forcing varies quickly over highly concentrated regions. The rheology is more important when the ice is more compact and stronger. Less compact ice responds quickly in both models under highly variable forcing conditions, since both models are in relatively free drift regimes, but highly compact ice experiences more inertia in the VP model. This lagged response is a direct result of linearizing the stress tensor term in the discretized form of (1). That is, the ice pack is not treated as a perfect viscoplastic material.

Poor temporal resolution of the forcing fields during the integration aggravates this problem. If the winds were steady, the VP model ice motion would eventually reach a steady state, and as long as the winds vary slowly, the VP model can maintain a sufficiently accurate transient response. In these simulations, the surface forcing fields are 3-day averages that have been linearly interpolated to the 4-h time step. The VP model does not reach steady state, but variations in the winds and currents generally occur slowly enough that long-time average effects on ice concentration and thickness fields are essentially the same in the two models.

Thus, the time step needs to be small enough to resolve the important physical timescales. On the other hand, it needs to be long enough that useful studies can be carried out with our current computational resources. The key is that we do not actually need to resolve the shortest timescale; we need only resolve those timescales that permit the ice to respond accurately to the relevant forcing timescale. We therefore perform a delicate balancing act, allowing a certain amount of error while trying to obtain a physically reasonable response to the forcing.

We have presented results for only the first year of integration. Our purpose was to investigate differences in the models' transient responses to the forcing and discuss how these differences will affect simulations of the Arctic climate. While the EVP model is considerably more accurate on shorter timescales, the two models produce similar ice distribution fields over the course of a year, and the effects on climate of the two different dynamics models can be expected to remain similar.

Finally, the EVP ice dynamics model significantly advances the computational efficiency of sea ice models for climate studies. Iterative methods used to integrate viscous-plastic models are slow, particularly on high-resolution grids, and they do not parallelize well. We have demonstrated that the EVP model can be multitasked quite easily and that it obtains superior performance on vector-parallel machines.

Acknowledgments. We thank John Dukowicz and Albert Semtner for their comments on and support of this investigation, and gratefully acknowledge support by the DOE CHAMMP Program and the NSF ARCSS Program for the Arctic System Study (YZ). Model simulations were performed on computers at the National Center for Atmospheric Research.

REFERENCES

Aagaard, K., and E. C. Carmack, 1989: The role of sea ice and other fresh water in the Arctic circulation. *J. Geophys. Res.*, **94,** 14 485–14 498.

Barry, R. G., M. C. Serreze, J. A. Maslanik, and R. H. Preller, 1993: The Arctic sea ice-climate system: Observations and modeling. *Rev. Geophys.*, **31,** 397–422.

Campbell, W. J., 1965: The wind-driven circulation of ice and water in a polar ocean. *J. Geophys. Res.*, **70,** 3279–3301.

Colony, R., and A. S. Thorndike, 1984: An estimate of the mean field of sea ice motion. *J. Geophys. Res.*, **89,** 10 623–10 629.

Hibler, W. D., 1979: A dynamic thermodynamic sea ice model. *J. Phys. Oceanogr.*, **9,** 817–846.

——, and J. E. Walsh, 1982: On modeling seasonal and interannual fluctuation of Arctic sea ice. *J. Phys. Oceanogr.*, **12,** 1514–1523.
——, and S. F. Ackley, 1983: Numerical simulation of the Weddell Sea pack ice. *J. Geophys. Res.*, **88,** 2873–2887.
——, and K. Bryan, 1987: A diagnostic ice-ocean model. *J. Phys. Oceanogr.*, **17,** 987–1015.
Hunke, E. C., and J. K. Dukowicz, 1997: An elastic-viscous-plastic model for sea ice dynamics. *J. Phys. Oceanogr.*, **27,** 1849–1867.
Kreyscher, M., M. Harder, and P. Lemke, 1997: First results of the Sea Ice Model Intercomparison Project (SIMIP). *Ann. Glaciol.*, **25,** 18–25.
Oberhuber, J. M., 1993a: Simulation of the Atlantic circulation with a coupled sea ice–mixed layer–isopycnal general circulation model. Part I: Model description. *J. Phys. Oceanogr.*, **23,** 808–829.
——, 1993b: Simulation of the Atlantic circulation with a coupled sea ice–mixed layer–isopycnal general circulation model. Part II: Model experiment. *J. Phys. Oceanogr.*, **23,** 830–845.
Parkinson, C. L., and W. M. Washington, 1979: A large-scale numerical model of sea ice. *J. Geophys. Res.*, **84,** 311–337.
Preller, R. H., and P. G. Posey, 1989: The Polar Ice Prediction System—A sea ice forecasting system. Tech. Rep. NORDA 212, Naval Research Laboratory, Stennis Space Center, MS, 42 pp. [Available from Naval Research Laboratory, Stennis Space Center, MS 39529-5004.]
Semtner, A. J., 1976: A model for the thermodynamic growth of sea ice in numerical investigations of climate. *J. Phys. Oceanogr.*, **6,** 379–389.
Steele, M., J. Zhang, D. Rothrock, and H. Stern, 1997: The force balance of sea ice in a numerical model of the Arctic Ocean. *J. Geophys. Res.*, **102,** 21 061–21 079.
Thorndike, A. S., and R. Colony, 1982: Sea ice motion in response to geostrophic winds. *J. Geophys. Res.*, **87,** 5845–5852.
Tremblay, L.-B., and L. A. Mysak, 1997: Modeling sea ice as a granular material, including the dilatancy effect. *J. Phys. Oceanogr.*, **27,** 2342–2360.
Yang, J., and J. D. Neelin, 1993: Sea–ice interaction with the thermohaline circulation. *Geophys. Res. Lett.*, **20,** 217–220.
Zhang, J., and W. D. Hibler, 1997: On an efficient numerical method for modeling sea ice dynamics. *J. Geophys. Res.*, **102,** 8691–8702.